Scaling of Ferrite-assisted Synchronous Reluctance Machines for Lifting Systems

Scaling of Ferrite-assisted Synchronous Reluctance Machines for Lifting Systems

Paolo Ragazzo
Dipartimento Energia Galileo Ferraris
Politecnico di Torino
Turin, Italy
paolo.ragazzo@polito.it

Simone Ferrari
Dipartimento Energia Galileo Ferraris
Politecnico di Torino
Turin, Italy
simone.ferrari@polito.it

Gaetano Dilevrano
Dipartimento Energia Galileo Ferraris
Politecnico di Torino
Turin, Italy
gaetano.dilevrano@polito.it

Lorenzo Beatrici
ITG Tecnologie S.r.l.
Rovereto, Italy
lorenzobeatrici@itgtecnologie.it

Christian Girardi
ITG Tecnologie S.r.l.
Rovereto, Italy
christiangirardi@itgtecnologie.it

Gianmario Pellegrino
Dipartimento Energia Galileo Ferraris
Politecnico di Torino
Turin, Italy
gianmario.pellegrino@polito.it

***Abstract*—This paper deals with the design and scaling of ferrite-assisted synchronous reluctance machines for lifting applications, to quickly obtain a family of motors from an initial reference design. A simple thermal network is introduced to describe the analysed non-ventilated motors. Thus, the scaling laws of the thermal network are also introduced, after calibration using the through heating test of the reference motor. The paper demonstrates how to scale the motor and converter size up or down to cover a wide range of lifting system applications. The turns versus length design plane is employed to select the correct number of turns and minimize the stack length of the scaled machine at the same time. Last, demagnetization, notably a downside of ferrite permanent magnets, is covered with dedicated magnetostatic simulations. Overall, the proposed design process aims at being a guideline for designing a series of e-motors in seamless computational time.**

***Index Terms*—AC machines, lifting systems, ferrite-assisted synchronous machines, scaling procedure.**

I. Introduction

As in many other fields, also lifting systems manufacturers aim at new motoring solutions to increase performance and reduce production costs [1]. The most challenging figures of merit in this field are passenger comfort, allowable load and travel speed, landing precision and low energy consumption [2]. The traditional systems, based on DC motors and induction motors (IM) do not satisfy the requirements of modern elevators [3]. Over the last decades, low-speed gearless permanent magnet synchronous motors (PMSM) based on rare-earth PMs have replaced the traditional systems thanks to their higher efficiency and compactness, associated with noise reduction and excellent control performance providing safety and comfort. However, rare-earth PMs are known for their price volatility and supply uncertainty; for example, neodymium had a peak increase of +300% between 2020 and 2022, as reported in Fig. 1 [4]. Other key raw materials of the NdFeB alloy such as Dysprosium, showed similar trends. On the other hand, the widely available, rare-earth free, ferrite magnets have notably a stable price over the years. As 90% of ceramic ferrite is made of ferrite oxide, this experienced a maximum rise of 30% during 2021 and 2022 [5]. Ferrite magnets have been employed in ferrite-assisted synchronous reluctance machines (PM-SyR) for lifting applications [6], home appliances [7] and traction [8] to enhance the performance of pure synchronous reluctance (SyR) machines with low impact on the cost. In [9], a PM-SyR machine is compared with a NdFeB PMSM to drive a gearless elevator system; the research demonstrated a 60% cost reduction thanks to the use of ferrite.

This paper targets ferrite-based gearless lift applications with direct drive connection to the elevator of lifting systems sheave. Such drives are characterized by low rotational speeds in the order of a few hundred rpm or lower, and correspondingly high torque values, and intermittent service [10]. The paper proposes a fast and accurate scaling method to cover a wide range of lifting applications starting from a single motor design in seamless computational time. Scaling laws are an established practice in the literature; reference [11] addresses the magnetic scaling of PMSMs stack diameter,

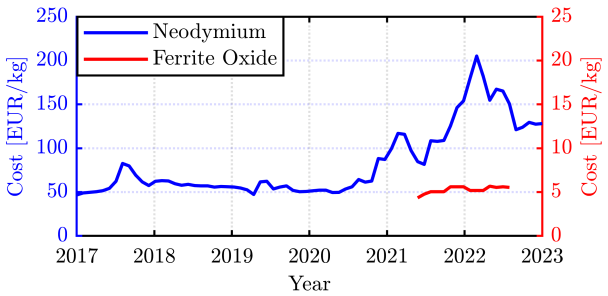

Fig. 1. Neodymium and ferrite oxide trends over time according to [4] [5]. Note that 90% of ceramic ferrite is made of ferrite oxide.

The present work is funded by ITG Tecnologie S.r.l, Rovereto, Italy and by the Power Electronics Innovation Center (PEIC) of Politecnico di Torino, Torino, Italy.

active length and number of turns. The flux map based scaling procedure previously proposed for traction application [12] included the freedom of choice of the inverter voltage and current, independently of dimensional scaling, and introduced the new turn-versus-length design plane and the law for scaling the steady-state thermal limit for the liquid cooling case. This paper extends this procedure to non-ventilated motors for lifting purposes. The proposed thermal model is experimentally calibrated for the reference machine and then scaled. The study is carried out using the open-source, Matlab and FEMM [13] based design platform SyR-e [14].

II. Reference Specifications and Baseline Motor

Reference is made to the per-unit requirements listed in Tab. I: Mot2 is the reference machine, existing and tested, whereas Mot1 and Mot3 are the down-scaled and up-scaled versions. Figs. 4-3 define the reference duty cycles for the three target lifting applications with different load and speed requirements.

A. Nominal Torque Definition

The design is carried out for the duty cycle displayed in Fig. 3. From the average temperature standpoint, the periodic duty cycle is equivalent to a continuous torque equal to rms torque value T_N, defined as (1).

$$T_N = \sqrt{\frac{1}{t_c}\int_0^{t_c} (T(t))^2\, dt} = \ 1 \text{ pu} \qquad (1)$$

Where t_c is the duty cycle period and t the variable time. Iron and PM loss effects are negligible, thanks to the low speed. Also, temperature undulation is negligible, due to the short duration of the cycle with respect to the thermal time constant of the non-ventilated machines. The T_N value of Mot2 is the base value for per unit normalization. Thus, according to the reference duty cycle in Fig. 3, the peak torque of Mot2 is 2.56 p.u.

TABLE I
Design Requirements.

			Mot1	Mot2	Mot3
Nominal torque	T_N	[pu]	0.58	1	1.5
Peak torque	T_{max}	[pu]	1.45	2.56	3.93
Inverter current	I_{max}	[pu]	0.78	1	1.67
DC voltage	V_{dc}	[pu]	1	1	1
Maximum speed	n_{max}	[pu]	0.66	1	1.05
Stator outer diameter	D	[pu]	0.87	1	1.2
Max stack length	L	[pu]	0.98	0.840	0.96
Shaft diameter	d_s	[pu]	0.22	0.280	0.32
Peak copper temperature	$\Theta_{Cu,max}$	[°C]	140	140	140

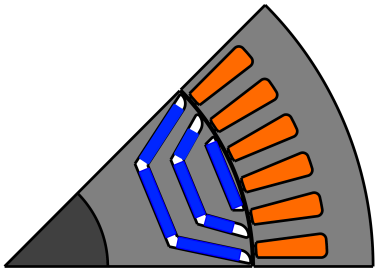

Fig. 2. PM-SyR motor example similar to the reference design. The ferrite magnets are highlighted in blue.

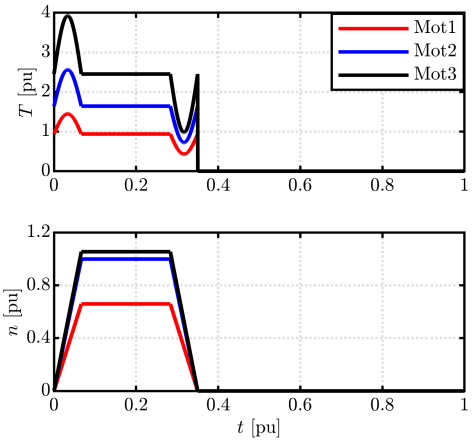

Fig. 3. Torque and speed vs time envelope over one reference duty cycle.

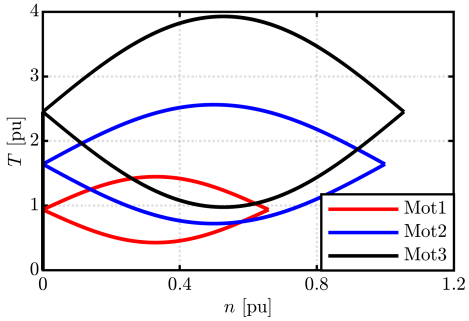

Fig. 4. Torque vs speed envelope over a reference duty cycle.

B. Reference Motor Design

The reference Mot2, an 8 poles and 48 slots PM-SyR motor, is represented in Fig. 2 and it was designed with the process presented in [15]. The barrier width and shape are adapted to use PM pieces of the same size as much as possible, as visible in Fig. 2. Regarding loss analysis, AC loss in copper are initially disregarded, as well as iron and magnet losses because of the low fundamental frequency (<10 Hz). Furthermore, the PWM impact on loss is not included due to high p.u. inductance and related low current ripple [16]. The loss breakdown of Mot2 at nominal torque is reported in Tab. II. Once again, it is evident that the high DC resistance and the low operating frequency make the AC loss contributions insignificant. The

TABLE II
Loss breakdown for the duty cycle point at maximum speed

DC Copper	AC copper	Iron and magnet
1 pu	$5 \cdot 10^{-5}$ pu	0.013 pu

loss analysis is conducted with the methodologies presented in [17].

C. Thermal Model Calibration

Ansys Motor-CAD [18] was used to evaluate the thermal performance of the reference motor (Mot2) in continuous operation and over repeated duty cycles (Fig. 3). The thermal model was built using datasheet properties of the motor materials and represents a non-ventilated, radially-finned housing. Then, the motor was manufactured and tested on a test rig (Fig. 5), where flux-map identification and a series of heating tests were executed. The fan visible in Fig. 5 was used to assess possible thermal improvements with ventilated cooling; this permits the examination of two options for different elevator requirements. The flux map measurements [7] match the simulation results obtained in SyR-e [14]. While the thermal measurements requested to apply correction factors to the starting thermal network, as largely done in literature [19]. The heating test results are reported in Fig. 6, was executed at a fixed current of 1 p.u. and the winding temperatures ($\Theta_{Cu,1}$ and $\Theta_{Cu,2}$) were read with thermocouples respectively in the end-winding and in the slots. After 65 minutes, the fan is switched ON producing a remarkable temperature drop, especially in the slots. Subsequently, the thermal model in Motor-CAD was corrected with reference to the temperatures measured on the first part of the test, corresponding to the fan OFF condition since the scaling process is performed with this thermal condition. Notice that the target was to repeat the reference duty cycle for 60 minutes without exceeding the 140°C limit for the winding. This requirement is fulfilled as conveyed by Fig. 7. Correction factors were applied to the convection coefficients to match the maximum copper and housing temperatures, as shown in Fig.7.

Once the thermal model was calibrated, it was used as a baseline for the scaling process by retrieving the maximum steady-state copper loss of the reference machine. In the following section, a simplified thermal network is constructed based on the calibrated Motor-CAD model; then thermal scaling rules are retrieved and applied to quickly estimate the thermal behaviours of the scaled motors.

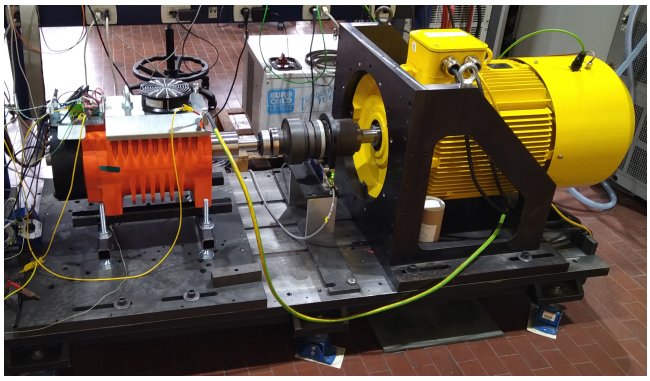

Fig. 5. Prototype of the reference machine Mot2 (left) mounted on the test rig.

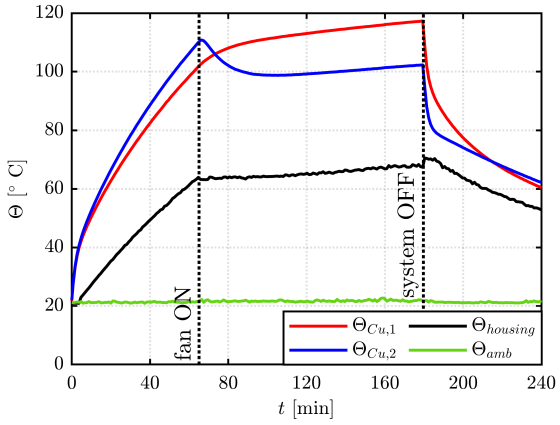

Fig. 6. Heating test with the fan OFF and ON with constant current reference: measured temperatures over time.

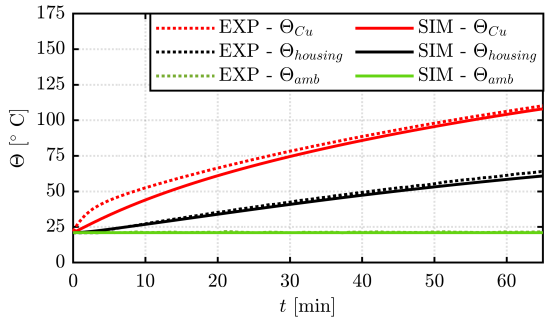

Fig. 7. Thermal model results after the calibration process on the convection factors according to the experimental tests.

III. Scaling Process

The following scaling factors are employed in the paper:

$$k_D = \frac{D}{D_0} \qquad k_L = \frac{L}{L_0} \qquad k_N = \frac{N_s}{N_{s0}} \tag{2}$$

They represent respectively the ratio of the outer stator diameter D, stack length L and number of turns in series N_s to the respective quantities of the reference machine Mot2, whose quantities are indicated in the following with 0.

A. Non-ventilated, scalable thermal model

The simplified thermal network of Fig. 8 is used to calculate the steady-state torque in stall condition (i.e. at 0 rpm). First, the baseline thermal network is retrieved upon the previously calibrated Motor-CAD model. Then, the thermal parameters are scaled with the laws described in the following.

The thermal resistance between iron and housing is expressed as (3) [20]. Similarly, the thermal resistance from housing to ambient is found as (4).

$$R_{Fe,h0} = \frac{2}{\pi\, h_{c,1}\, L\, D} \tag{3}$$

$$R_{h,amb0} = \frac{2}{\pi\, h_{c,2}\, L\, D_{hous}} \tag{4}$$

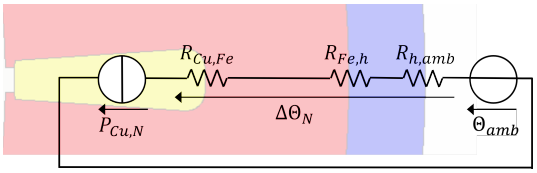

Fig. 8. Simplified thermal network for non-ventilated machines.

where $h_{c,1}$ and $h_{c,2}$ are the core to housing and housing to ambient convection heat transfer coefficients, respectively [21].

Thus, the baseline thermal resistance between copper and iron can be retrieved from the thermal network (Fig. 8) as (5).

$$R_{Cu,Fe0} = \frac{\Delta\Theta_{N0}}{P_{Cu,N0}} - R_{Fe,h0} - R_{h,amb0} \tag{5}$$

where $\Delta\Theta_{N0}$ is the maximum temperature rise of copper with respect to ambient temperature, defining the nominal copper loss $P_{Cu,N0}$. Applying the scaling factors (2) to the thermal resistance equations (3) (4) (5), the corresponding scaling rules are found:

$$\frac{R_{Cu,Fe}}{R_{Cu,Fe0}} = \frac{1}{k_L} \tag{6}$$

$$\frac{R_{Fe,h}}{R_{Fe,h0}} = \frac{R_{h,amb}}{R_{h,amb0}} = \frac{1}{k_L k_D} \tag{7}$$

Note that the thermal scaling laws are defined assuming the convection heat transfer h_c to be independent of the stack dimensions. Imposing that the allowed copper to ambient temperature rise is the same for all the machines, the nominal copper loss at stall of the scaled machine is calculated (8).

$$\frac{P_{Cu,N}}{P_{Cu,N0}} = \frac{R_{Cu,Fe0} + R_{Fe,h0} + R_{h,amb0}}{R_{Cu,Fe} + R_{Fe,h} + R_{h,amb}} \tag{8}$$

B. Diameter Ratio and Length-turns scaling plane

In this paper, the diameter ratio k_D is prescribed and follows the nominal torque rating. In machines of higher speed, the diameter size can be determined after the maximum speed constraint [12] or by other considerations.

Fixed the diameter, the selection of k_L and k_N is addressed using the length-turns plane displayed in Fig.11 and Fig. 9. The plane refers to maximum torque per ampere (MTPA) conditions and shows the peak torque (at maximum inverter current) with blue contours and the base speed at maximum inverter voltage with red contours, function of the axial length and number of turns scaling factors (k_L, k_N).

The construction of the length-turns plane is based on the manipulation of the MTPA curves of the reference machine, consisting of the dq current and flux linkage components function of torque, retrieved numerically by manipulation of the flux linkage maps. Indeed, the MTPA curves of the reference machine are scaled accordingly to the magnetic scaling law [11] and queried at the peak operating point of the target inverter. It must be remarked that the length-turns scaling plane is fully analytical and thus it takes less than a second to be retrieved with standard laptops; another valuable point is that the scale laws are accurate and do not contain any approximations. However, it must be highlighted that the scaling laws are valid if the radial cross-section is entirely scaled according to the diameter scaling factor, as done in this paper: thus, the airgap and ribs must be scaled accordingly to k_D. However, in the scale-down process, the resulting airgap or the rotor ribs could be too small and not mechanically acceptable. In this case, further FEA would be needed with the adjusted airgap or ribs.

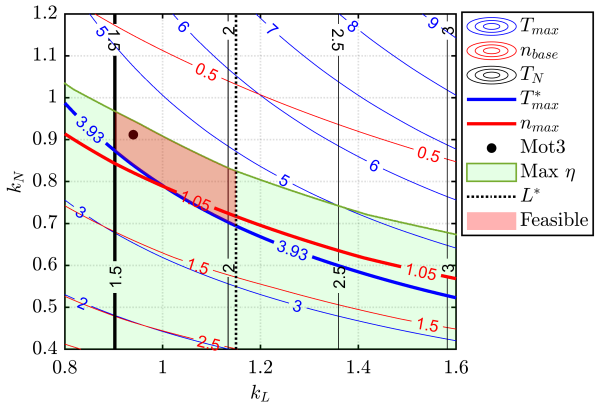

Fig. 9. Length-turns scaling plane according the Mot3 requirements.

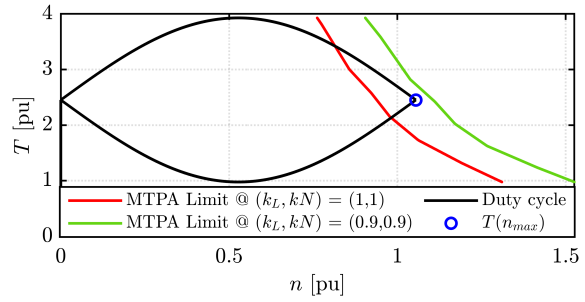

Fig. 10. Duty cycle of Mot3 and MTPA speed limits function torque for two example machines.

As usual for lifting systems, the motors are required to not work in flux-weakening, in order to improve the system efficiency. For this reason, the design target is to cover the duty cycles in Fig. 4 only in MTPA conditions, without going into the flux-weakening region.

This requirement is contemplated in the scaling plane as highlighted in Fig. 10. In this figure, the points of the reference duty cycle are reported on the torque-speed plane in black, together with the MTPA limits for two examples on the plane, reported in red and green respectively. If a working point falls above the MTPA limit, flux weakening occurs for the considered design. It follows that the maximum efficiency is fulfilled for a specific (k_L, k_N) configuration if all the operating points of the duty cycle lay below the MTPA limit curve, as for green line in Fig. 10. This condition is fulfilled for all the designs highlighted with a green area over the scaling plane in Fig. 9 and 11. Thanks to the scaled MTPA law, it is

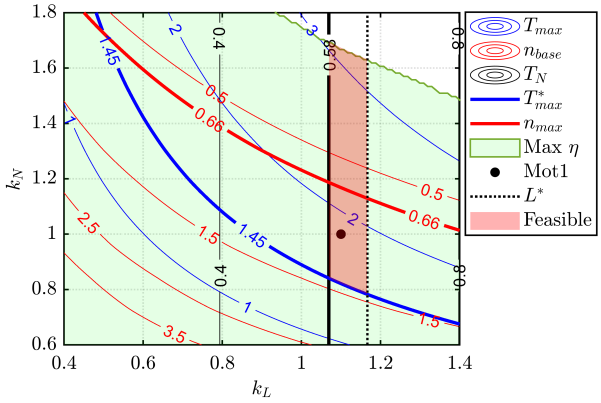

Fig. 11. Length-turns scaling plane according the Mot1 requirements.

possible, for each point in this area, to check if the reference duty cycle can be covered in MTPA condition and fulfilling the inverter limits. To better explain this behaviour, two points are selected from the plane in Fig. 9 and their MTPA limits are reported in Fig. 10. Here, the red line indicates a motor that has to operate in flux-weakening to cover part of the cycle, whilst the green line represents a motor that can fully cover the cycle in MTPA. The area below the curve can be covered in MTPA condition, while above the MTPA limit, the motor can not cover the operating points or need flux weakening, with given inverter limits.

Another quantity reported with black contours on the plane is the rated torque T_N, retrieved from the calibrated thermal model described before and imposing the target copper temperature.

IV. Case Study

A. Scale up: Mot3

The scaling plane of Mot3 is shown in Fig. 9 and it is built upon the reference motor by applying the prescribed diameter scaling factor of 1.2. The crucial figures of merit are plotted as contours with reference to MTPA operation, as disclosed in the previous section. The only MTPA or maximum efficiency area described in the previous section is coloured in green. Moreover, the feasible area must account also for other constraints, reported in (9), where the targets and limits are reported with the apex *. These constraints are the peak torque, rated torque (computed with the calibrated thermal network) and stack length limit. The area where all these conditions are fulfilled is reported in red, and the final scaled design must be selected within this red area.

$$\begin{cases} T_{max} > T^*_{max} \\ T_N > T^*_N \\ T(n_{max}) \in \text{MTPA} \\ L < L^* \end{cases} \tag{9}$$

The scaled design is chosen on the left side of the feasible area to minimize the stack length ($k_L = 0.94$). Furthermore, a rewinding factor corresponding to a feasible number of turns is selected ($k_N = 0.91$).

From the scaling plane, is evident that the thermal requirements (i.e. the rated torque T_N) set a limit for stack length reduction. Moreover, with respect to the reference motor, the radial scaling increases torque itself, allowing a stack length reduction compared to the reference motor and also compared to the stack length limits.

B. Scale down: Mot1

The Mot1 scaling process starts, as the previous one, with the target diameter requirements that impose a k_D equal to 0.85. Thus, the scaling plane is constructed with reference to the target inverter and reported in Fig. 11. The plane shows that the two magnetic requirements in (9) (peak torque and maximum efficiency) are fulfilled in a wide area of the plane. Indeed, a stack length scaling factor of around 0.5 would ensure the target peak torque and no flux weakening on the target cycle. However, the continuous torque imposes a minimum k_L of around 1.1, demonstrating that the thermal requirement represents a considerable bottleneck of these specification sets. Moreover, the feasible area, corresponding to the condition (9) and highlighted in red in Fig. 11, is vertically wide, communicating that a smaller inverter could have been used. Finally, the Mot1 is placed at k_N equal to 1, to simplify the manufacturing process, indeed, in this way the Mot1 and Mot2 have the same winding configuration, even if with different wire cross-sections. Also, the minimum stack length scaling factor is chosen within the feasible area, which corresponds to 1.1.

C. Qualification of Mot1 and Mot3

At this stage, the design of Mot1 and Mot3 is completed with the analysis of the demagnetization limit and the thermal assessment under the prescribed duty cycle by means of the Motor-CAD models, which also validate the simplified thermal network results.

The demagnetizing current evaluation is performed by iteratively searching for the current value that demagnetizes 1% of PM volume. In Fig. 12 the demagnetizing currents for the three

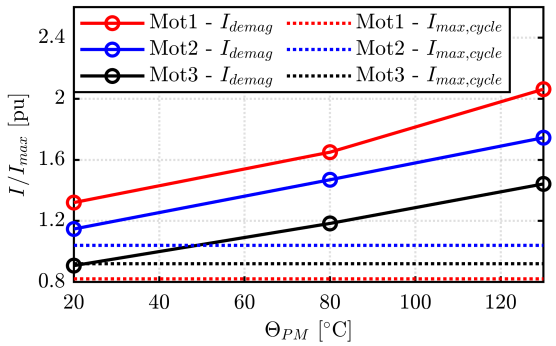

Fig. 12. Demagnetizing currents vs PM temperature. Dashed lines indicate the maximum current requested over the duty cycles. Note that here 1pu corresponds to the maximum inverter current of each motor.

TABLE III
MOTORS COMPARISON.

			Mot1	Mot2	Mot3
Target nominal torque	T_N^*	[pu]	0.58	1	1.5
Nominal torque	T_N	[pu]	0.59	1	1.55
Target peak torque	T_{max}^*	[pu]	1.45	2.56	3.93
Peak torque	T_{max}	[pu]	1.82	2.56	4.27
Max stack length	L^*	[pu]	0.98	0.84	0.96
Stack length	L	[pu]	0.92	0.84	0.76
Number of turns	N_s		272	272	248

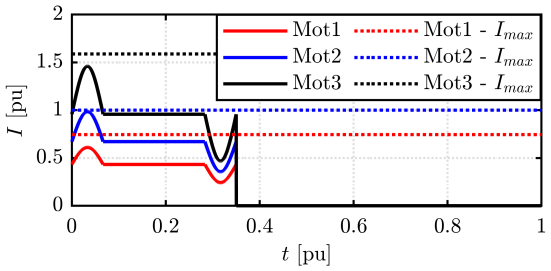

Fig. 13. Current required over the duty cycles and inverter current limits.

motors are reported with reference to the respective inverter current rating. The motors are safe against demagnetization at the rated temperature. The most critical motor is the Mot3, which, for low temperatures, has the maximum current over the cycle close to the demagnetizing current.

Tab. III reports the scaling process outcome and it compares the resulting performance with the initial requirements; here, good margins on the stack length and on the peak torque can be appreciated. The nominal torque reported in Tab. III is computed with Motor-CAD, through the calibrated thermal model. This rated torque is identified through an iterative process, that ensures a maximum copper temperature equal to the target of 140°C, as from Tab. I.

Fig. 13 shows the minimum current rating required to cover the reference duty cycles for each machine. Here, it is possible to notice that Mot1 does not exploit all the inverter current capability (as already observed in its length-turns plane) and then an inverter downsizing could be evaluated. A stack length reduction is not possible since there is no margin on the continuous torque because of the strict thermal limit.

V. CONCLUSION

This paper proposes a comprehensive and straightforward scaling procedure to build a series of electric motors for lifting applications. Firstly, the reference design is introduced and experimentally identified. The scaled motor dimensions and output figures are determined using a comprehensive approach based on the flux maps of the initial machine. In particular, the length-turns design plane is used to detect the optimal length and turns combination, with reference to four figures of merit: peak torque, base speed, no-flux weakening needed in the reference duty cycle and continuous torque. Then, a thermal network is proposed and its scaling rules are offered. Last, the procedure is tested on scaled-up and scaled-down versions of the reference machine. The two scaled machines show perfect agreement with the respective torque and speed requirements, and the thermal network estimations match well with the more complex Motor-CAD model.

ACKNOWLEDGMENT

The research is the outcome of the joint work between ITG Tecnologie S.r.l. and Power Electronics Innovation Center (PEIC) of Politecnico di Torino.

REFERENCES

[1] R. Anand and M. Mahesh, "Analysis of elevator drives energy consumptions with permanent magnet machines," in *2016 IEEE Smart Energy Grid Engineering (SEGE)*, 2016, pp. 186–190.
[2] J. Wang, F. Tan, and R. Jin, "Research on low-speed gearless permanent magnet synchronous motor for elevator drive," in *2005 International Conference on Electrical Machines and Systems*, vol. 1, pp. 454–459.
[3] O. V. Kruglikov, "Low-speed induction motors for directly driven elevator machines," vol. 86, pp. 118–124.
[4] TRADING ECONOMICS | 20 million INDICATORS FROM 196 COUNTRIES. [Online]. Available: https://tradingeconomics.com/
[5] P. Fears. Ferrite magnet price trends. [Online]. Available: https://www.bunting-berkhamsted.com/ferrite-magnet-price-concerns/
[6] B. Boazzo, A. Vagati, G. Pellegrino, E. Armando, and P. Guglielmi, "Multipolar ferrite-assisted synchronous reluctance machines: A general design approach," vol. 62, no. 2, pp. 832–845.
[7] E. Armando, R. I. Bojoi, P. Guglielmi, G. Pellegrino, and M. Pastorelli, "Experimental identification of the magnetic model of synchronous machines," vol. 49, no. 5, pp. 2116–2125.
[8] S. Jurkovic, K. Rahman, B. Bae, N. Patel, and P. Savagian, "Next generation chevy volt electric machines; design, optimization and control for performance and rare-earth mitigation," in *2015 IEEE Energy Conversion Congress and Exposition (ECCE)*. Montreal, QC, Canada: IEEE, Sep. 2015, pp. 5219–5226.
[9] H. Yetiş, E. Meşe, and M. Biyikli, "Design and comparison of ferrite based IPM and NdFeB based SPM synchronous motors for gearless elevator systems," in *2018 XIII International Conference on Electrical Machines (ICEM)*, pp. 635–641, ISSN: 2381-4802.
[10] K. Al-Kodmany, "Tall buildings and elevators: A review of recent technological advances," vol. 5, no. 3, pp. 1070–1104.
[11] S. Stipetic, D. Zarko, and M. Popescu, "Ultra-fast axial and radial scaling of synchronous permanent magnet machines," in *2016 IET Electric Power Applications*.
[12] G. Dilevrano, P. Ragazzo, S. Ferrari, G. Pellegrino, and T. Burress, "Magnetic, thermal and structural scaling of synchronous machines," in *2022 IEEE Energy Conversion Congress and Exposition (ECCE)*, pp. 1–8, ISSN: 2329-3748.
[13] D. Meeker, "FEMM: Finite element method magnetics." [Online]. Available: www.femm.info
[14] F. Cupertino and G. Pellegrino. SyR-e. [Online]. Available: https://github.com/SyR-e
[15] P. Ragazzo, G. Dilevrano, S. Ferrari, and G. Pellegrino, "Design of IPM synchronous machines using fast-FEA corrected design equations," in *2022 International Conference on Electrical Machines (ICEM)*, pp. 1–7, ISSN: 2381-4802.
[16] A. Hava, R. Kerkman, and T. Lipo, "Simple analytical and graphical methods for carrier-based pwm-vsi drives," *IEEE Transactions on Power Electronics*, vol. 14, no. 1, pp. 49–61, 1999.
[17] S. Ferrari, P. Ragazzo, G. Dilevrano, and G. Pellegrino, "Flux and Loss Map Based Evaluation of the Efficiency Map of Synchronous Machines," *IEEE Transactions on Industry Applications*, pp. 1–10, 2022.
[18] Ansys motor-CAD | electromechanical design software. [Online]. Available: www.ansys.com/en-gb/products/electronics/ansys-motor-cad
[19] C. Sciascera, P. Giangrande, L. Papini, C. Gerada, and M. Galea, "Analytical thermal model for fast stator winding temperature prediction," vol. 64, no. 8, pp. 6116–6126.
[20] A. Boglietti, A. Cavagnino, and D. Staton, "Determination of critical parameters in electrical machine thermal models," vol. 44, no. 4, pp. 1150–1159.
[21] P. Mellor, D. Roberts, and D. R. Turner, "Lumped parameter thermal model for electrical machines of TEFC design," vol. 138, no. 5, p. 205.